Computers in Biology and Medicine 110 (2019) 93–107

Contents lists available at ScienceDirect

Computers in Biology and Medicine

journal homepage: www.elsevier.com/locate/compbiomed

A self-organized recurrent neural network for estimating the effective connectivity and its application to EEG data

Zahra Abbasvandi, Ali Motie Nasrabadi*

Department of Biomedical Engineering, Faculty of Engineering, Shahed University, Tehran, Iran

ARTICLE INFO

Keywords:
Effective connectivity
Recurrent neural network
Granger causality
Self-organized network
Epileptic seizures

ABSTRACT

Objective: Effective connectivity is an important notion in neuroscience research, useful for detecting the interactions between regions of the brain.
New method: Since we are dealing with a dynamic system, it seems that using a dynamic tool could effectively achieve better results. In this paper, a novel approach, called "Recurrent Neural Network - Neuron Growth Using Error Whiteness - Granger Causality" (RNN-NGUEW-GC) is proposed to estimate the effective connectivity. An RNN is used for predicting and modeling time series and multivariate signals. NGUEW is used to determine the optimum time lag with the help of an error whiteness criterion. When this criterion is not satisfied, the number of neurons in the network input is increased, producing an increase in the time lag. Accordingly, the network achieves a self-organized structure. Finally, causal effects are determined for linear and nonlinear models using the concept of Granger causality. Also, an indicator of the "intensity of causality" is defined to approximate the strength of the linear interactions based on the structure of the network and the weights of the connections.
Conclusions: RNN-NGUEW-GC had a major outcome in terms of both method accuracy on simulation data and prediction of epileptic seizures on the EEG dataset. The main advantages of this method in comparison with other methods of determining the effective connectivity are: 1) there is no need for physiological information; 2) it yields a self-organized network structure. In addition, the calculation of the appropriate time lag using NGUEW is another superiority of this method in comparison with multivariate auto-regressive models.

1. Introduction

One of the most complicated natural systems is the human brain. There are still a myriad of unknowns about the functionality of the brain even after long study of this topic. In recent years, the purpose of most studies has been identifying the specific relations between the tasks of the brain and the regions of the brain [1]. The importance of the "brain integration concept" has guided most studies in the direction of brain connectivity [1]. Generally, there are three types of brain connectivity: structural connectivity, functional connectivity, and effective connectivity [2]. The concept of effective connectivity deals with the causal effect of one region of the brain on another [3]. Effective connectivity analysis is useful because neurologists can identify abnormal behavior of the brain, such as Alzheimer's syndrome [4], autism [5], and epilepsy [6,7], based on the changes these disorders induce in these causal relations. In addition, they can determine effective treatments for these disorders.

Many computational methods have been used to represent the effective connectivity of the brain, such as Dynamic Causal Models (DCMs) [8] and Structural Equation Models [9]. These methods require an anatomical model and physiological information, which is their most important drawback. Nevertheless, there are other methods for this purpose, such as Granger causality (GC) [10]. Multivariate GC-based methods are all fundamentally based on Multivariate Auto-Regressive (MVAR) models. Even though in MVAR models physiological information is not required, there are still some limitations. For example, the structure and order of the model should be determined initially and then used to calculate the effective connectivity. In addition, Dynamic Bayesian Network (DBN) models have been used to determine the effective connectivity. To simplify the problem, DBN considers only one previous sample of data for estimating the effective connectivity [11–13].

Calculating the effective connectivity using an artificial neural network (ANN) has recently drawn a great deal of attention. For example, Talebi et al. [14] proposed CREANN, which uses a multilayer perceptron neural network for estimating the effective connectivity. Khadem et al. [15] suggested the βmRMR-MLP-GC model to identify direct nonlinear effective connectivity using multilayer perceptron

* Corresponding author.
E-mail address: nasrabadi@shahed.ac.ir (A.M. Nasrabadi).

https://doi.org/10.1016/j.compbiomed.2019.05.012
Received 26 September 2018; Received in revised form 12 May 2019; Accepted 12 May 2019

neural networks. This model involves the estimation of causal relations between EEG channels based on the concept of GC.

Although the results of the mentioned papers are satisfactory and can be considered as an estimation of the causal links between brain regions, they nevertheless have a few drawbacks. Firstly, the network structure should be determined in the first step. Secondly, it has been discovered that there are receiver connections between brain regions which are inconsistent with feedforward neural networks [16]. That article showed that the cerebral cortex executes a hypothetical reasoning in response to sensory inputs. In other words, the cerebral cortex collects more information from input sensory signals through processing information from the top layers and sending it to the bottom layers using efferent nerves in addition to processing information from the down layers to the top layers using afferent nerves, to make the initial hypothesis as close as possible to the reality of the things in the world. Therefore, it seems a recurrent neural network (RNN) would outperform a feedforward neural network because the structure of a recurrent network is significant from biological point of view. The RNN model has been used successfully for predicting and modeling time series and EEG signals [17,18].

The present paper proposes the use of RNN models instead of feedforward neural networks for estimating the effective connectivity. In addition, detection of the time lag is done via the Neuron Growth Using Error Whiteness (NGUEW) algorithm. NGUEW checks the whiteness of the error at specific times. When the training error is not white, the number of neurons in the network input is increased, which adds a time lag to the system. Then, a combination of RNN and NGUEW is employed. This combination is combined with the concept of GC to provide a new method, called RNN-NGUEW-GC, to estimate the effective connectivity. Finally, the existence of causal effects is determined for linear and nonlinear models. Also, an indicator of the "intensity of causality" is defined in order to approximate the strength of linear interactions. This method is applied to both simulated datasets and experimental EEG data.

Fig. 1 demonstrates the process of the method. Since the analysis of brain function has evolved significantly during the last decades and a variety of methods addressing effective connectivity are currently available, the proposed method can be used along with other methods for calculating the effective connectivity. Also, it can reveal the strength and the intensity of the information flow between regions of the brain.

RNN-NGUEW-GC does not require an anatomical model or physiological information. In addition, this method is not like DBN, which considers only one previous sample. Indeed, there is no predefined parameter for the time lag. Instead, it is calculated automatically based on NGUEW, and the network structure is determined as a self-organized structure. These features are the most important superiorities of this method over auto-regressive (AR) methods. Besides, a self-organized RNN is a dynamic neural network with recurrent connections and a self-correcting character, inspired by the brain [16]. Therefore, a self-organized RNN can operate well in recognizing the activities of the brain, and it is used as a computational model in neuroscience. The goal of such models in neuroscience is the identification of brain functions, cognitive behaviors, and to show how the nervous system analyzes information. In addition, the effectiveness and performance of the proposed neural network led us to apply the method to the task of prediction. Using RNN for effective connectivity estimation and NGUEW for determining the proper time lag constitute the innovations of this paper.

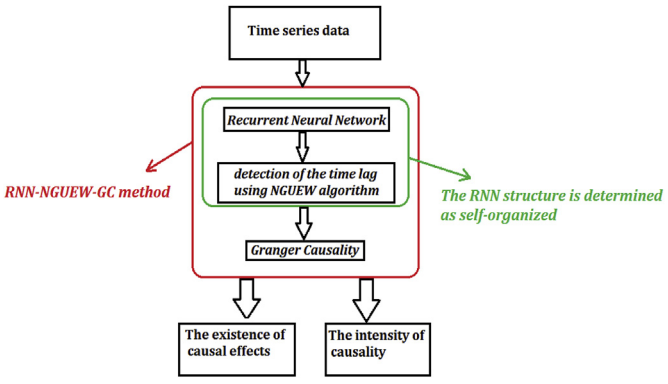

Fig. 1. The process of the proposed method: RNN is used for predicting and modeling time series. NGUEW is used to determine the optimum time lag. GC is used to estimate the effective connectivity.

The structure of this paper is as follows: in Section 2, we present a short overview of the previous studies. Section 3 describes the computational methods used in this paper including the structure of the RNN, the NGUEW algorithm, and the concept of GC. In Section 4, we combine these three computational methods and present the proposed method (RNN-NGUEW-GC). In Section 5, we report the results of applying RNN-NGUEW-GC to the simulated and the EEG datasets. In Section 6, we discuss the results. Section 7 presents our conclusions and some proposals for further research.

2. Review

This part provides a general review of the previous studies in each of the following categories:

- Effective connectivity (see Section 2.1)
  Effective connectivity is usually described as the causal influence that one system exerts over another and reveals the direction of the information flow between regions of the brain.
- Recurrent neural networks (see Section 2.2)
  RNN is a powerful tool that has been successfully employed in many applications, such as predicting and modeling time series and EEG signals [17,18].

2.1. Effective connectivity

Physiological evidence can inform the development of models that explain how regions of the brain interact with each other. The theoretical concepts of these interactions are the foundation for model-based effective connectivity. This technique can evaluate hypotheses and physiological models. Friston et al. [8] introduced Dynamic Causal Model (DCM) for fMRI, and then this idea was generalized to EEG and MEG data [19,20]. DCM has been used to investigate effective connectivity, employing resting state functional magnetic resonance imaging data [21]. Also, Xiang et al. [22] proposed a local adjustment model-based approach, L-DCM. This model quantifies the effective connectivity between different regions of the brain in epileptic seizures.

In contrast to model-based methods, there are other methods, such as GC, which can determine the effective connectivity of the brain without physiological information [10]. Granger introduced a linear mathematical model derived from Winner causality theory [23]. GC is one of the most popular concepts with which to study the causal influence of time series. It has been applied in economics and neuroscience because of its simplicity, understandability, and easy implementation [24]. In 2012, the Granger Multivariate Autoregressive Connectivity (GMAC) toolbox was described in Ref. [25]. The toolbox can study connectivity using Granger causality analysis on fMRI images. Multivariate GC-based criteria have been introduced in the time domain, such as the Conditional Granger Causality Index [26], and in the frequency domain, such as DTF, dDTF, ffDTF, and PDC [27,28].

Since the interactions between signals can be nonlinear, different methods have been proposed for nonlinear GC. In 2003, an information-theoretic test for general GC was used to identify nonlinear couplings [29]. Researchers have introduced measures of nonlinear effective connectivity by defining Kernel Granger Causality (KGC) [30]. KGC is a parametric measure, and its performance depends on the kernel

used. In addition, it is a bivariate measure, thus, it may not identify the direct and indirect connections. To solve this issue, a multivariate version of KGC has been proposed [31,32]. Farokhzadi et al. [33] developed another method for measuring nonlinear effective connectivity, called ANFICGC. By this method, the existence of linear and nonlinear connections was detected. However, the intensities of the interactions were not obtained.

There is another method which calculates the effective connectivity with the help of transfer entropy, first proposed by Marko [34]. This method needs to estimate probability distribution functions [35]. Transfer entropy was applied to capture the magnitude of information flow [36]. In that study, normalized transfer entropy was localized and was regularized to avoid unstable results.

In recent years, the possibility of a proper mapping from input to output in ANNs as a nonlinear and adaptive method along with the outstanding features of ANN has made it useful for estimating the effective connectivity of the brain [14,15]. Due to the benefits of ANNs, a computational model from resting state fMRI data was proposed in Ref. [37]. This simulation is based on brain activation, which is a direct reflection of cortical connectivity.

2.2. Recurrent neural networks

Due to the “universal approximation theorem,” an accurate approximation of any function can be achieved from one neural network with one hidden layer and a sufficient number of hidden neurons [38]. As the mandatory conditions for this theorem, the hidden-layer activation function must grow steadily and be limited, nonlinear, and continuous. RNN is a subset of ANNs with the “universal approximation” property. RNNs are biologically inspired tools because of the existence of recurrent connections in the brain, which are used to break down different problems, such as time series prediction [39].

Among several proposed structures for RNNs, partially recurrent neural networks (PRNNs) have attracted a great deal of attention. In comparison with fully recurrent neural networks, PRNNs have the advantage of more organized recurrent links, thereby accelerating learning and causing fewer stability problems. The Jordan neural network [40], which uses feedback from the output layer, along with Elman neural networks [41], which have information fed back from the hidden layer, are two major types of PRNN for modeling dynamic systems. Researchers have proposed a NARX neural network based on the Jordan model [42]. This model was able to capture the nonlinear activities of fMRI data. Wang et al. [43] developed the Jordan-plus Elman NARX recurrent neural network and proposed its training procedure.

RNNs are very complicated due to the existence of recurrent links. Therefore, the training process may be time-consuming. To solve this problem, we can optimize the network structure. One of the ways of optimizing the network structure is the use of growing and pruning algorithms [44]. An adaptive growing and pruning algorithm which can add to or prune the hidden neurons to reduce the computational complexity and improve the generalization performance was presented in Ref. [45].

3. Computational methods

During the last decade, scientific research focusing on brain connectivity has increased and many methods have been developed. In this section, we explain the computational methods used in this paper including the structure of the RNN, the growth of the neural network with the NGUEW algorithm, and the GC index.

3.1. The structure of the RNN

The structure of the network demonstrated in Fig. 2a is composed of an input layer, an output layer with an equal number of neurons, and one hidden layer, involving recurrent connections between its neurons. Several neurons are embedded in each layer. These neurons are completely connected to other neurons in the previous layer and the next layer. The structure of the neuron is displayed in Fig. 2b. An activation function f is applied to the weighted sum of inputs of each neuron plus a bias term to generate the output of the neuron. By taking f to be a nonlinear function (such as the lag-sigmoid function or the tan-sigmoid function), the concept of nonlinearity is injected into the neural network to provide a powerful model which is similar to a biological system. Network parameters (weights) are estimated with the help of training data. The quality of the training is evaluated using validation data and the network is tested by calculating the error on a test dataset.

3.2. Number of input time lags

According to Fig. 2a, all inputs are imported to the system with delays (1, 2, 3 …, p) and different weights; therefore, we consider p as the time lag of this system.

The model order can be identified by applying traditional methods such as Schwarz's Bayesian Criterion and the Akaike Information Criterion [46–48]. Also, different methods, such as the Mutual Information technique, have been developed [14], from the function approximation point of view, with the aim of selecting the appropriate inputs of an ANN.

In this research, we used the neuronal growth technique to detect p. The growth of the number of neurons helps us determine the time lag based on an automatic criterion without operator interference. It contributes to developing a self-organized network structure, which is the main advantage of this method in comparison with AR-fitting.

In the execution phase, we trained the network continuously until the validation error starts to increase. At that time, training was stopped and the whiteness of the training error was checked. Error whiteness is one of the important conditions in model validation [49]. Accordingly, we used this criterion for automatic detection of p. Indeed, the main criterion of the growth algorithm for making a decision about the growth of neurons is checking the whiteness of the error. When the condition of error whiteness is not satisfied, neurons are added into the input layer of the network. The input of each new neuron represents the previous time lag of the same channel. After adding neurons, we trained the network and then repeated the previous steps again. Accordingly, this procedure adds input delays to the network if required. This approach towards determining the time lag for the network by adding neurons is called the Neuron Growth Using Error Whiteness (NGUEW) algorithm and is described in Fig. 3.

In this figure, *Number_GN* denotes the number of grown neurons. The rest of the variables have been defined in Fig. 2. If the training error is not white, the neuron will grow in the input layer as large as the number of main inputs, with the initial weights of grown neurons selected randomly. Therefore, according to this approach, the time lag is determined and the network structure is obtained as self-organized. The RNN structure for two inputs and two stages of growth is illustrated in Fig. 4.

3.3. Granger causality index (GCI)

Assume that two AR models of $x(t)$ and $y(t)$ are being measured in parallel, and let $e(t)$ denote the forecast error of $x(t)$ when $x(t)$ is the result of a linear combination of p previous samples of $x(t)$ (see Eq. (1)).

$$x(t) = \sum_{i=1}^{p} A(i)x(t-i) + e(t) \tag{1}$$

From the other side, $e'(t)$ is the forecast error when $x(t)$ is the result of a linear combination of p previous samples of $x(t)$ and q previous samples of $y(t)$ (see Eq. (2)).

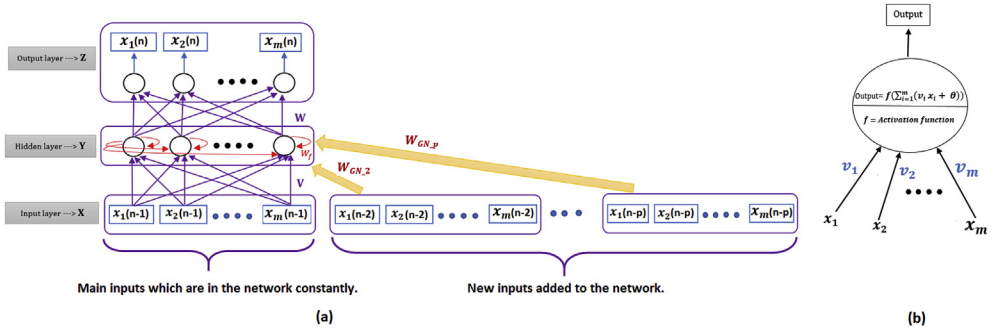

Fig. 2. (a) The RNN structure with one hidden layer; there are recurrent connections between the neurons of this layer. (b) The structure of a neuron: an activation function is applied to the weighted sum of inputs of each neuron along with a bias term to generate the output of the neuron.

$$x(t) = \sum_{i=1}^{p} A(i)x(t-i) + \sum_{j=1}^{q} B(j)y(t-j) + e'(t) \tag{2}$$

Accordingly, Eq. (3) is the Linear Granger Causality (LGC) measure from y to x. If GCI_{yx} is a significantly positive value, a linear causal influence from y to x will be inferred [50].

$$GCI_{yx} = \ln\left(\frac{e(t)^2}{e'(t)^2}\right) \tag{3}$$

4. Proposed method

In this section, we propose the RNN-NGUEW-GC method, which is a mixture of RNN modeling, the NGUEW algorithm, and the theory of GC. Consider m EEG channels, denoted by $x_M(n)$; $M = 1. \ldots. m$; $n = 1. \ldots.L$. The time series data are divided into three separate parts: the training data (x_M^{train}) with a length of L_1 (almost 70% of the samples); validation data (x_M^{Valid}) with a length of L_2 (almost 15% of the samples); and testing data (x_M^{test}) with a length of L_3 (almost 15% of the samples). In order to estimate every channel $x_M(n)$ using the RNN-NGUEW-GC method, the data are fed into RNN for training. The error on the validation data is monitored during the training phase. The validation error normally decreases during the initial step of training. As soon as the network begins to overfit the training data, the error on the validation data starts to rise. When the validation error increases for a specified number of epochs (valid_fail = 10), the training stops. Then, the error whiteness is checked. When the error is white, we accept the training and use the weights the network had in the valid_fail = 10 previous steps as the result of running the training; otherwise, the number of neurons grows and a time lag is added to the network. Fig. 5 presents the flowchart of this algorithm.

Eq. (4) represents the calculation of the Mean Squared Error (MSE) of the validation data. In this equation, $z_{valid}(n)$ is the estimate of $x_{valid}(n)$.

$$MSE_{valid} = \sqrt{\frac{\left(\sum_{n=1}^{L_2}\left(x_{valid}(n) - z_{valid}(n)\right)^2\right)}{L_2}} \tag{4}$$

Finally, the prediction error of each input and optimum weights are obtained by executing this method. The GC is calculated using the training error. Here, it is determined whether there is a causal effect from each channel to the others or not (see Section 4.1). Also, the

A. ***Initialization:*** *p =1;*
Number_GN=0; (the initial number of grown neurons)

B. ***Training:*** *Input of network: X(n-1);*
Desired output of network: X(n). So Z(n) is an estimation of X(n).

if p =1 →
- $Z(n) = W * Y(n)$;
- $Y(n) = Tanh(V * X(n-1) + W_f * Y(n-1))$;
- *Weights are updated with the BPTT algorithm.*

if $p \geq 2$ →
- $Z(n) = W * Y(n)$;
- $Y(n) = Tanh(V * X(n-1) + \sum_{i=2}^{p} W_{Gn\_i} * X(n-i) + W_f * Y(n-1))$;
- *Weights are updated with the BPTT algorithm.*

C. ***Checking the condition for stopping the training (early stopping method):***

If *the stop condition isn't satisfied:*
Goto (B)

If *the stop condition is satisfied:*
Goto (D)

D. ***Checking the error whiteness:***

If *the error is not white:*
Number_GN= Number_GN+m; (m=the number of main inputs)
Initial weights of grown neurons (W_{Gn_i})*= random ;*
p =p +1; (time lag adds to the network)
Goto (B)

If *the error is white:*
We accept the training.

Fig. 3. Neuron Growth Using Error Whiteness (NGUEW) algorithm; the main criterion of this algorithm is checking the error whiteness. When the condition of error whiteness is not satisfied, the number of neurons grows in the input layer of the network. The input of each new neuron is the previous time lag of the same channel. Accordingly, this procedure adds input delays to the network.

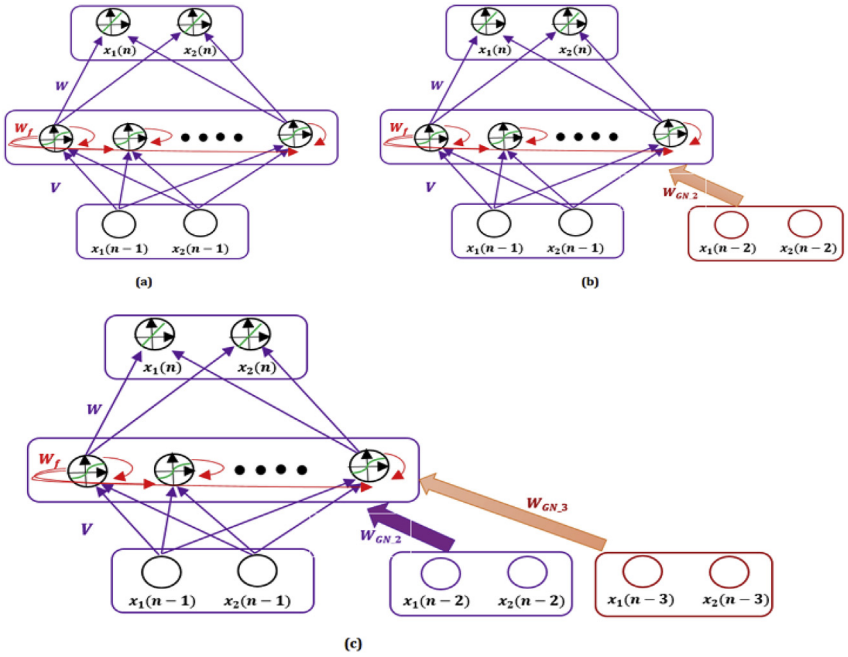

Fig. 4. (a) The Network structure (b) The network structure after one stage of growth; with one stage of growth, a second delay is entered into the system. (c) The network structure after two stages of growth; with this stage of growth, a third delay is entered into the system, also.

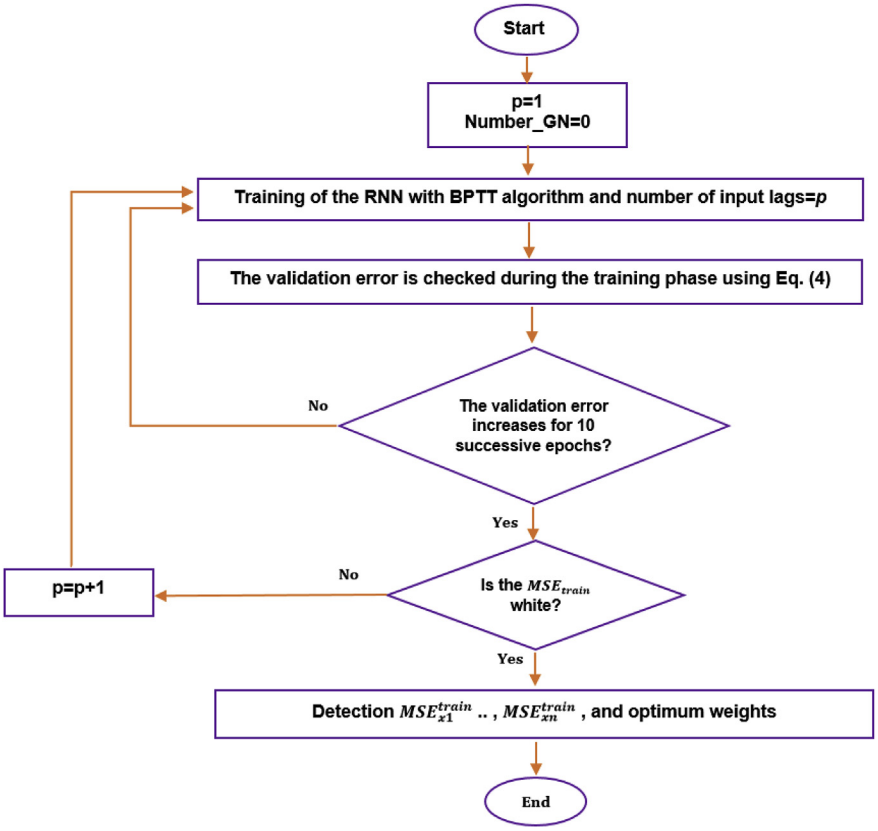

Fig. 5. The flowchart of the proposed method for finding the optimum weights and MSE of training data; the validation error is monitored during the training phase. When the validation error increases, the training stops and the error whiteness is checked. When the error is white, we accept the training.

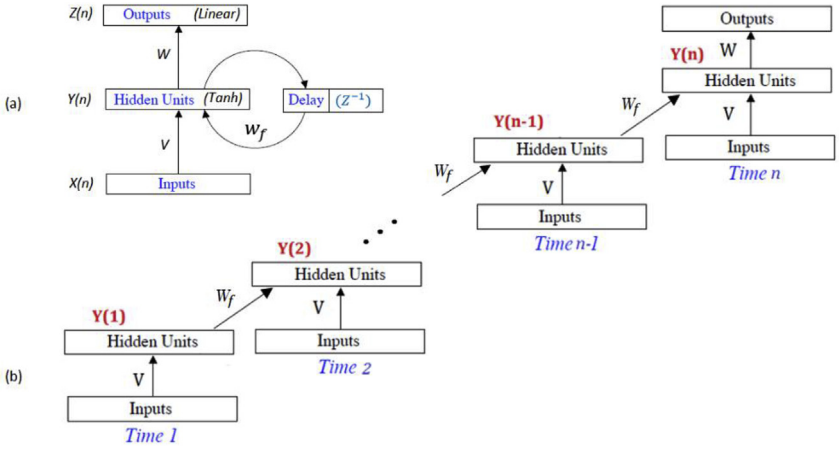

Fig. 6. (a) The general structure of the network (b) "Unfolding" of the recurrent network over time.

indicator of "intensity of causality" is defined in order to estimate the strength of the linear interactions (see Section 4.2).

4.1. The existence of causal effects

With the help of the GC-based criteria used in Ref. [15], the causal link between channels was investigated based on Eq. (5).

$$GC_{x_1 \to x_2} = \ln\left(\frac{MSE_{x_2}^{train-Ch_2}}{MSE_{x_2}^{train-Ch_1 \& Ch_2}} \right) \tag{5}$$

Suppose that we have two channels. With the help of this criterion, initially, we train the neural network with the information of both channels 1 and 2 to identify the prediction error of x_2 ($MSE_{x_2}^{train-Ch_1 \& Ch_2}$) and optimum weights. Then, in order to investigate the effect of channel 1 on channel 2, we deactivate channel 1, and by the same weights obtained from the previous step, the prediction error of x_2 ($MSE_{x_2}^{train-Ch_2}$) is calculated again. A causal link from x_1 to x_2 exists if $GC_{x_1 \to x_2}$ is significantly positive; otherwise, the mentioned link is not available. The significance of $GC_{x_1 \to x_2}$ is tested by an adequate number of generated surrogate data (see the Appendix).

4.2. The intensity of causality

The indicator of "intensity of causality" represents the strength of the linear interactions. To calculate this index, the overall structure of the network has been assumed to be as in Fig. 6a.

The mathematical relation between the input and output is defined by Eq. (6).

$$Y(n) = Tanh(VX(n) + W_f\, Y(n-1))$$

$$Z(n) = WY(n)$$

If the function ***Tanh*** (.) is approximated by its first term of the Taylor series [14], we have Eq. (7).

$$Tanh(VX(n) + W_f\, Y(n-1)) \approx VX(n) + W_f\, Y(n-1) \tag{7}$$

We unfold RNN as shown in Fig. 6b and consider $Y(n-1)$ as a function based on the previous values of X (see Eq. (8)).

$$\boldsymbol{Y}(1) \cong \boldsymbol{VX}(1)$$

$$Y(2) \cong VX(2) + W_f\, Y(1) \to \boldsymbol{Y}(2) = \boldsymbol{Vx}(2) + \boldsymbol{W_f}\, \boldsymbol{VX}(1)$$

$$Y(3) \cong VX(3) + W_f\, Y(2) \to Y(3) \cong Vx(3) + W_f\, (Vx(2) + W_f\, VX(1)) \to$$

$$\boldsymbol{Y}(3) \cong \boldsymbol{Vx}(3) + \boldsymbol{W_f}\, \boldsymbol{Vx}(2) + \boldsymbol{W_f^2}\, \boldsymbol{VX}(1))$$

.....

$$Y(n) \cong Vx(n) + W_f\, Y(n-1) \to Y(n) \cong Vx(n) + W_f\, VX(n-1) + W_f^2 VX(n-2) + W_f^3 VX(n-3) + \ldots + W_f^{n-1} VX(1)$$

$$\to \boldsymbol{Y(n)} \cong \boldsymbol{Vx(n)} + \sum_{\boldsymbol{k=1}}^{\boldsymbol{n-1}} \boldsymbol{(W_f)^k\, VX(n-k)}$$

For this network with N_i inputs, N_h nonlinear neurons, and N_o linear outputs unit, we can write Eq. (9).

$$Y_l(n) \cong \sum_{m=1}^{N_i} \left(V_{ml} X_m(n) + \sum_{q=1}^{N_h} \sum_{k=1}^{n-1} \left(W_{f_{ql}}\right)^k V_{ml} X_m(n-k) \right); \quad l = 1{:}\, N_h \tag{9}$$

By transferring Eq. (9) to the Z domain, we have

$$Y_l(z) \cong \sum_{m=1}^{N_i} \left(V_{ml} X_m(z) + \sum_{q=1}^{N_h} \sum_{k=1}^{n-1} \left(W_{f_{ql}}\right)^k V_{ml}\, X_m(z) z^{-k} \right); \quad l = 1{:}\, N_h \tag{10}$$

$$Y_l(z) \cong \sum_{m=1}^{N_i} \left(V_{ml} X_m(z) + V_{ml} X_m(z) \sum_{q=1}^{N_h} \sum_{k=1}^{n-1} \left(W_{f_{ql}}\, z^{-1} \right)^k \right); \quad l = 1{:}\, N_h \tag{11}$$

$$Y_l(z) \cong \sum_{m=1}^{N_i} \left(V_{ml} X_m(z) + V_{ml} X_m(z) \sum_{q=1}^{N_h} \frac{W_{f_{ql}}\, z^{-1} - \left(W_{f_{ql}}\, z^{-1} \right)^n}{1 - W_{f_{ql}}\, z^{-1}} \right);$$

$$l = 1{:}\, N_h \tag{12}$$

Since $0 < w_f < 1$, we can skip $\left(W_{f_{ql}}\, z^{-1} \right)^n$, hence we have Eq. (13).

$$Y_l(z) \cong \sum_{m=1}^{N_i} V_{ml} X_m(z) \left(1 + \sum_{q=1}^{N_h} \frac{W_{f_{ql}}\, z^{-1}}{1 - W_{f_{ql}}\, z^{-1}} \right); \quad l = 1{:}\, N_h \tag{13}$$

Finally, the relation between the input and output is calculated by Eq. (14).

$$Z_s(z) \cong \sum_{l=1}^{N_h} W_{ls}\, Y_l(z); \quad s = 1{:}\, N_o \tag{14}$$

Using Eq. (13), we have

$$Z_s(z) \cong \sum_{l=1}^{N_h} W_{ls} \sum_{m=1}^{N_i} V_{ml} X_m(z) \left(1 + \sum_{q=1}^{N_h} \frac{W_{f_{ql}}\, z^{-1}}{1 - W_{f_{ql}}\, z^{-1}} \right); \quad s = 1{:}\, N_o \tag{15}$$

Table 1
The parameters of RNN-NGUEW-GC method as well as their settings for the simulation data and EEG data.

Category	Parameter	Settings
Growth parameters	***p*:** The number of input time lags of each time series at the beginning of training.	1
The RNN modeling parameters	***Activation function*:** The activation functions used by the neurons of each layer	Hidden layer: tan-sigmoid Out layer: Linear
	***Training algorithm*:** The algorithm used for training the RNN	BPTT
	***Valid_fail*:** Governs when the training is stopped and the condition for growth is checked.	10
Parameters of the significance testing	***Surrogate number*:** The number of generated surrogate datasets	1000
	P_{valu}**:** The threshold of P_{valu} for statistical significance testing	0.05

$$Z_s(z) \cong \sum_{m=1}^{N_i}\sum_{l=1}^{N_h}\left(W_{ls}V_{ml}\left(1+\sum_{q=1}^{N_h}\frac{W_{f_{ql}}z^{-1}}{1-W_{f_{ql}}z^{-1}}\right)\right)X_m(z);\quad s=1{:}\,N_o \tag{16}$$

Then, the "intensity of causality" that links the inputs to outputs is obtained with Eq. (17). This Equation represents the magnitude of the influence of the *m*th input node on the *s*th output neuron.

$$intensity\ of causality_{ms}=\sum_{l=1}^{N_h}\left(W_{ls}V_{ml}\left(1+\sum_{q=1}^{N_h}\frac{W_{f_{ql}}z^{-1}}{1-W_{f_{ql}}z^{-1}}\right)\right);$$
$$m=1{:}\,N_i;\quad s=1{:}\,N_o \tag{17}$$

The proposed RNN-NGUEW-GC method has multiple variables set according to Table 1. Note that the surrogate data parameters are the same as the parameters used in the original data.

5. Experimental results

In this part, we present the results of applying RNN-NGUEW-GC to both simulated datasets and EEG data. Matlab R2016a was used for the RNN modeling. In Section 5.1, we show the performance of RNN-NGUEW-GC on three different models of the simulated data and evaluate the proposed method. In Section 5.2, we use an invasive EEG signal to determine whether the proposed method has the ability to extract the iEEG signal behavior for seizure prediction.

5.1. Simulated data

Some simulation models were employed to evaluate the performance of the proposed RNN- NGUEW-GC method. We investigated different time series generated from an autoregressive process with 7000 samples, where σ_i $(i = 1.\ 2.\ 3)$ is the standard normal distribution with zero mean. The performance of the method was also investigated on a nonlinear and multivariate system. The values of the parameters used for the analysis of the simulated data were reported in Table 1.

5.1.1. Model with unidirectional interaction

Consider Eq. (18). The x_1 and x_2 variables were achieved after the autoregressive operation. In this simulation, an extreme asymmetry was generated, which indicated a unidirectional flow from x_2 to x_1 . This one-sided flow caused an asymmetric connectivity. In this model, x_1 is a function of its own past at time lag 1 (the auto term) and the past of x_2 at time lags 4 and 5 (the cross terms). Also, x_2 is a function of its own past at time lags 4 and 5.

$$\begin{aligned} x_1(n) &= 0.1\ x_1(n-1) - 0.3\ x_2(n-5) - 0.4\ x_2(n-4) + \sigma_1(n)\\ x_2(n) &= 0.5\ x_2(n-5) + 0.1\ x_2(n-4) + \sigma_2(n) \end{aligned} \tag{18}$$

Using Eq. (5), the existence of causal effects is displayed in Fig. 7. The significance of the causal effects was tested by the generated surrogate data. A causal link was available only when the calculated GC for the original data was larger than the threshold.

The "intensity of causality" calculation using Eq. (17) is provided in Table 2. These results suggest that Eq. (17) can estimate the strength of linear interactions with a low error.

5.1.2. Time-varying model

This section evaluates the performance of the proposed method (RNN-NGUEW-GC) to describe causal links of a case with time-varying coefficients. Consider the following time-varying model (Eq. (19)):

$$\begin{aligned} x_1(n) &= 0.3\,x_1(n-2) + 0.5\ x_2(n-2) + \sigma_1(n)\\ x_2(n) &= 0.5\ x_1(n-2) + C\ x_1(n-1) + \sigma_2(n) \end{aligned} \tag{19}$$

In this equation, C is the influence of $x_1(n-1)$ on x_2 , which is described by Eq. (20). (L is the length of the simulated data.)

$$C(n) = \begin{cases} 0.8 & n \le 0.3L \\ 0.2 & n > 0.3L \end{cases} \tag{20}$$

Eq. (5) was computed on the mentioned system, with the results demonstrated in Fig. 8. In addition, the statistical results of the introduced index are provided in Table 3.

The length of the data segment reached 200 points via dividing the data into $N = 35$ non-overlapping segments and choosing $L = 7000$. The model was assumed stationary in each segment. Fig. 9 exhibits the original value of C (solid line) which changes quickly (as a step function), with the estimated coefficient of C (blue dashed line) tracking this sudden change with a small error.

5.1.3. Nonlinear and multivariate model

If the interaction between signals is nonlinear and more than two signals are considered, the model will grow in complexity. In this section, we show that the proposed method is applicable to a nonlinear and multivariate system. Eq. (21) is an example of a nonlinear and multivariate model.

$$\begin{aligned} x_1(n) &= 0.2\,x_1(n-1)\,e^{-x_1(n-1)} + \sigma_1(n)\\ x_2(n) &= 0.5\ x_2(n-1) + 0.6\ x_1(n-1) + \sigma_2(n)\\ x_3(n) &= 0.2\,x_3(n-1)\,(1-x_3(n-1)) + 0.4\ x_2(n-1)e^{-x_2(n-1)} + \sigma_3(n) \end{aligned} \tag{21}$$

The investigation of causal effects is illustrated in Fig. 10. Based on Fig. 10, no indirect effect is found in the multivariate model. Thus, the proposed method resolves the drawbacks of some previous studies [51].

The indicator of "intensity of causality" represents the strength of linear interactions. In order to use this indicator for a nonlinear system, the strength of linear interactions should be extracted from the Taylor series. One expects that the value of estimated coefficients with the indicator of "intensity of causality" will essentially approach the real values, which are the output of the Taylor series (see Table 4).

5.2. EEG data

Epileptic seizure is one of the most common neurological disorders that are related to the electrical function of the brain. A sudden seizure can put the patient in a dangerous situation. Accordingly, predicting an epileptic seizure is significantly important for epileptic patients. It gives the patients enough time to prepare themselves against dangerous conditions; for example, they can stop while driving, call for help, or not cross a street. Therefore, the prediction of epileptic seizures is a major issue in neuroscience, since it may increase the quality of the life of a patient suffering from epilepsy.

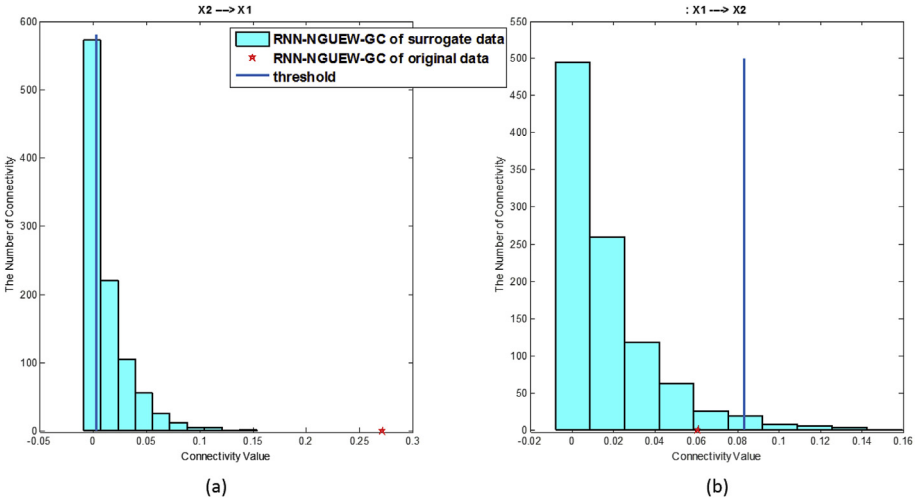

Fig. 7. Histogram of RNN-NGUEW-GC for surrogate data and original data related to model with unidirectional interaction; red star: the original data connectivity; blue line: the threshold. (a) Investigation of the existence of $\boldsymbol{x}_2 \rightarrow \boldsymbol{x}_1$ connection; the original data connectivity was greater than the threshold; therefore, there was a causal coupling from $\boldsymbol{x}_2$ to $\boldsymbol{x}_1$. (b) Investigation of the existence of $\boldsymbol{x}_1 \rightarrow \boldsymbol{x}_2$ connection; the original data connectivity was smaller than the threshold; therefore, there was no causal coupling from $\boldsymbol{x}_1$ to $\boldsymbol{x}_2$.

Table 2
The original and estimated coefficients of the model.

Intensity of Causality *(IoC)*	$\boldsymbol{IoC}_{\boldsymbol{x}1(\boldsymbol{n}-1)\rightarrow\boldsymbol{x}1}$	$\boldsymbol{IoC}_{\boldsymbol{x}1(\boldsymbol{n}-1)\rightarrow\boldsymbol{x}2}$	$\boldsymbol{IoC}_{\boldsymbol{x}2(\boldsymbol{n}-5)\rightarrow\boldsymbol{x}1}$	$\boldsymbol{IoC}_{\boldsymbol{x}2(\boldsymbol{n}-5)\rightarrow\boldsymbol{x}2}$	$\boldsymbol{IoC}_{\boldsymbol{x}2(\boldsymbol{n}-4)\rightarrow\boldsymbol{x}1}$	$\boldsymbol{IoC}_{\boldsymbol{x}2(\boldsymbol{n}-4)\rightarrow\boldsymbol{x}2}$
Original value	0.1	0	−0.3	0.5	−0.4	0.1
Estimated value	*0.11 ± 0.005*	*0.02 ± 0.004*	*−0.27 ± 0.006*	*0.53 ± 0.004*	*−0.39 ± 0.003*	*0.12 ± 0.003*

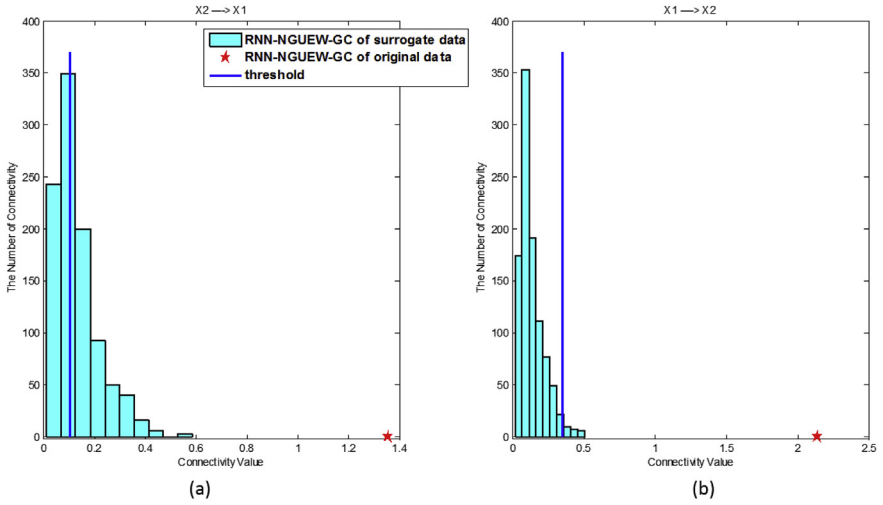

Fig. 8. Histogram of RNN-NGUEW-GC for surrogate data and original data related to time-varying model; red star: the original data connectivity; blue line: the threshold. (a) Investigation of the existence of $\boldsymbol{x}_2 \rightarrow \boldsymbol{x}_1$ connection (b) Investigation of the existence of $\boldsymbol{x}_1 \rightarrow \boldsymbol{x}_2$ connection; in both cases, the original data connectivity was greater than the threshold; therefore, there was a causal coupling from $\boldsymbol{x}_2$ to $\boldsymbol{x}_1$ and from $\boldsymbol{x}_1$ to $\boldsymbol{x}_2$.

Table 3
The original and estimated coefficients of the time-varying model.

Intensity of Causality *(IoC)*	$\boldsymbol{IoC}_{\boldsymbol{x}1(\boldsymbol{n}-2)\rightarrow\boldsymbol{x}1}$	$\boldsymbol{IoC}_{\boldsymbol{x}1(\boldsymbol{n}-2)\rightarrow\boldsymbol{x}2}$	$\boldsymbol{IoC}_{\boldsymbol{x}2(\boldsymbol{n}-2)\rightarrow\boldsymbol{x}1}$	$\boldsymbol{IoC}_{\boldsymbol{x}2(\boldsymbol{n}-2)\rightarrow\boldsymbol{x}2}$	$\boldsymbol{IoC}_{\boldsymbol{x}1(\boldsymbol{n}-1)\rightarrow\boldsymbol{x}1}$	$\boldsymbol{IoC}_{\boldsymbol{x}1(\boldsymbol{n}-1)\rightarrow\boldsymbol{x}2}$
Original value	0.3	0.5	0.5	0	0	C
Estimated value	*0.35 ± 0.01*	*0.62 ± 0.05*	*0.53 ± 0.04*	*0.07 ± 0.01*	*0.06 ± 0.005*	$\tilde{C}$

The Freiburg EEG database 2007 [52] has been used in this study to evaluate the performance of the proposed method. This dataset contains invasive EEG (iEEG) recordings of 21 patients suffering from focal epilepsy. So, in this study, the term EEG is employed instead of the term iEEG. The data was recorded at the Epilepsy Center of the University Hospital of Freiburg. In this study, the proposed method was applied to five of the patients of the Freiburg EEG database. This data was acquired on 128 channels and at a 256 Hz sampling rate, but practically only 6 channels out of 128 channels are available. Therefore, in this study, the proposed method was applied on these 6 channels only.

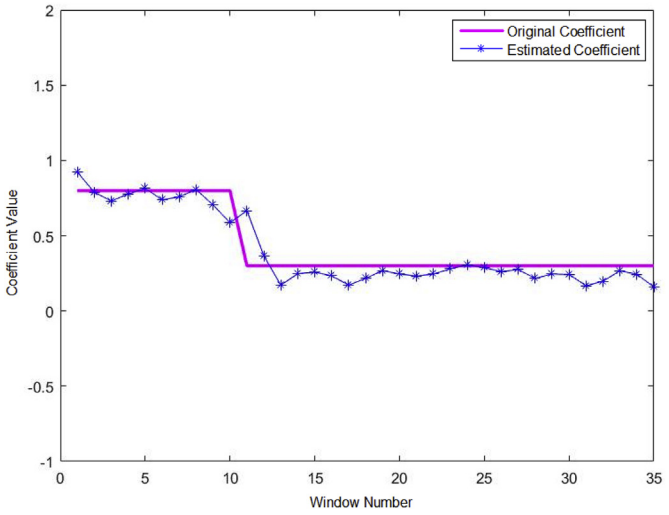

Fig. 9. The coefficient C, which is the influence of x_1 (n - 1) on x_2 (n); the estimated coefficient ($\tilde{C}$) is represented by the blue dashed line. The estimated coefficient (blue dashed line) tracks the original value (solid line) with a small error.

For each patient, there were two different datasets, called “ictal” and “interictal”. “Ictal” contained epileptic seizures and a minimum of 54 min of preictal data, while “interictal” included around 24 h of recorded EEG data without seizure activity. Since only six channels of the Freiburg EEG database were available, the structure of RNN would be a multivariate model with six inputs and six outputs. In this study, to reduce the calculation time, 10 h of “interictal” data were employed. Also, the length of the EEG segments that are assumed stationary is 5 s.

In this method, the time lag was determined automatically, by applying the growth algorithm to the “interictal” data. The minimum value achieved for the time lag on the investigated patients was 5. Then, by calculating Eq. (5) between each pair of channels, 36 features were obtained. Therefore, each feature indicates the connectivity between six channels. This process was applied to both the “ictal” data and the “interictal” data of each patient. Fig. 11 and Fig. 12 present the connectivity variations between six channels for “ictal” data and “interictal” data related to patient number 8.

For predicting epileptic seizures using EEG signal processing, two indexes were defined:

Table 4
The original and estimated coefficients of the model.

Intensity of Causality *(IoC)*	Original value	*Estimated value*
$IoC^{Linear}_{x1(n-1)\rightarrow x1}$ss	0.2	0.17 ± 0.06
$IoC^{Linear}_{x1(n-1)\rightarrow x2}$	0.6	0.62 ± 0.04
$IoC^{Linear}_{x1(n-1)\rightarrow x3}$	0	0.04 ± 0.05
$IoC^{Linear}_{x2(n-1)\rightarrow x1}$	0	0.02 ± 0.04
$IoC^{Linear}_{x2(n-1)\rightarrow x2}$	0.5	0.56 ± 0.07
$IoC^{Linear}_{x2(n-1)\rightarrow x3}$	0.4	0.38 ± 0.04
$IoC^{Linear}_{x3(n-1)\rightarrow x1}$	0	-0.01 ± 0.02
$IoC^{Linear}_{x3(n-1)\rightarrow x2}$	0	0.03 ± 0.03
$IoC^{Linear}_{x3(n-1)\rightarrow x3}$	0.2	0.21 ± 0.05

1) Sensitivity: The ratio of successful predictions to the number of total seizures (see Eq. (22))
2) False positive rate (FPR): The average number of false predictions per hour (see Eq. (23))

$$Sensitivity = \frac{Number\ of\ true\ positives}{Number\ of\ true\ positives + Number\ of\ false\ negatives} \quad (22)$$

$$FPR = \frac{Number\ of\ false\ positives}{Time\ in\ hours} \quad (23)$$

A few thresholds were also defined in order to evaluate the FPR and sensitivity. These thresholds were generated using Eq. (24) and varying i from 1 to 200. In this equation, the mean and standard deviation (δ) were related to the first hour of “interictal” data connectivity for each patient. These thresholds were defined for triggering an alarm.

$$Th = mean \pm i\,(\delta) \quad ; \quad 1 \le i \le 200 \quad (24)$$

Fig. 13 shows the prediction threshold for 1 out of 36 connectivities as a sample. In this case, lower threshold values (Th3) led to better sensitivity, since more seizures can be predicted properly with acceptable FPR. A very high dependency is visible between sensitivity and FPR in every prediction method.

The following two time intervals are important for epileptic seizure prediction:

1) Seizure Prediction Horizon (SPH) is the duration in which there is no seizure.

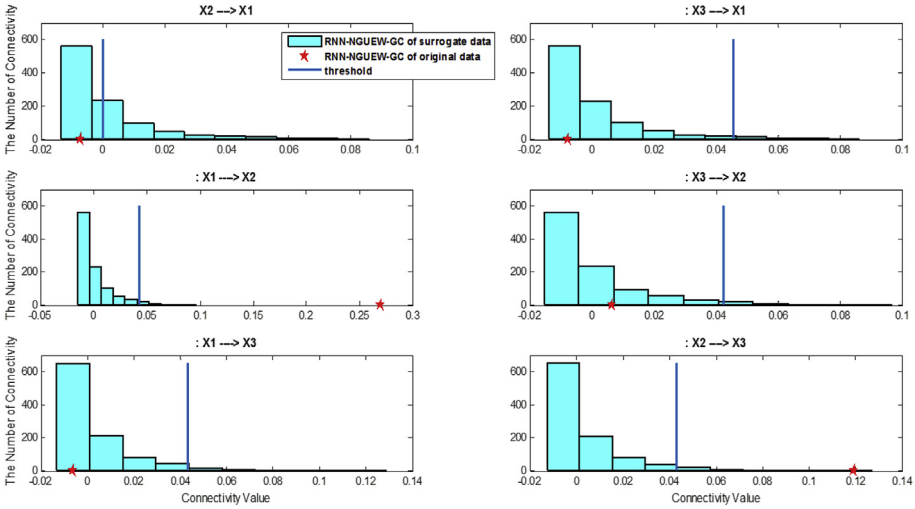

Fig. 10. Histogram of RNN-NGUEW-GC for surrogate data and original data related to a nonlinear model; red star: the original data connectivity; blue line: the threshold. When the original data connectivity is greater than the threshold, it is concluded that there is a causal coupling; otherwise, there is no causal coupling.

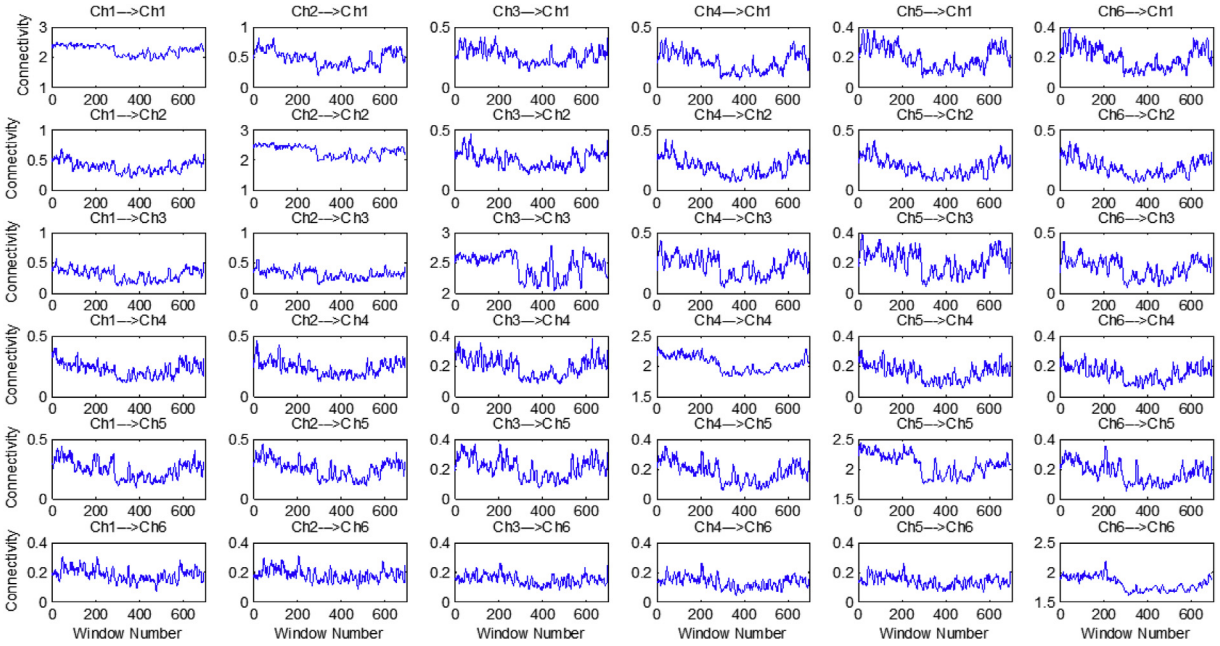

Fig. 11. The connectivity variations among six channels for "ictal" data from patient number 8; features were defined based on the effective connectivity, so 6 channels lead to 36 features. In addition to the intensity of interactions, their direction is also important.

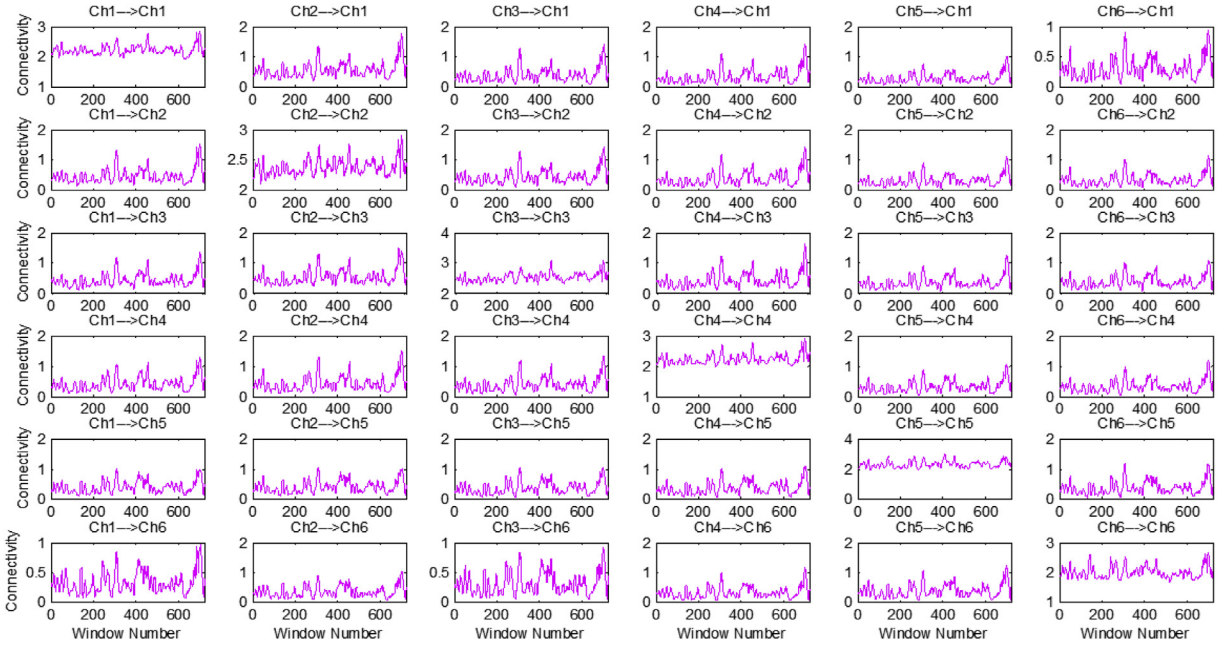

Fig. 12. The connectivity variations among six channels for "interictal" data from patient number 8.

2) Seizure Occurrence Period (SOP) is the time interval in which we are sure a seizure has occurred.

In an optimistic situation, the SPH is long and SOP is short. In this study, the SOP and SPH were considered to be 40 and 20 min, respectively.

Fig. 14 illustrates our approach for decision-making in order to predict epileptic seizures. In this approach, a moving window is used. Using the moving window, a few samples from the EEG data are received for analysis every time (Fig. 14a). The output of this analysis is a new variable known as "Counter." In order to calculate the value of "Counter," Eq. (5) was applied to each pair of channels, whereby 36 connectivities were obtained for each window (Fig. 14b). "Counter" is equal to the total number of connectivities passing the threshold, in each window. Then, this variable will be compared with a criterion: if it is greater than the criterion, the alarm will be triggered (Fig. 14c). The optimum criterion obtained in this study was 5. Again, by moving the window, another sample from the EEG data will be received, this procedure will be repeated, and "Counter" will be calculated for the next window.

In this study, the triggering of an alarm means that a seizure onset must occur after the SPH and within the SOP, for a correct prediction. So, any wrong prediction leads to an increase in the FPR, while correct predictions cause higher sensitivity. Accordingly, in order to test the accuracy of the method, the mentioned prediction approach was applied to both the "ictal" and the "interictal" data. Table 5 shows the

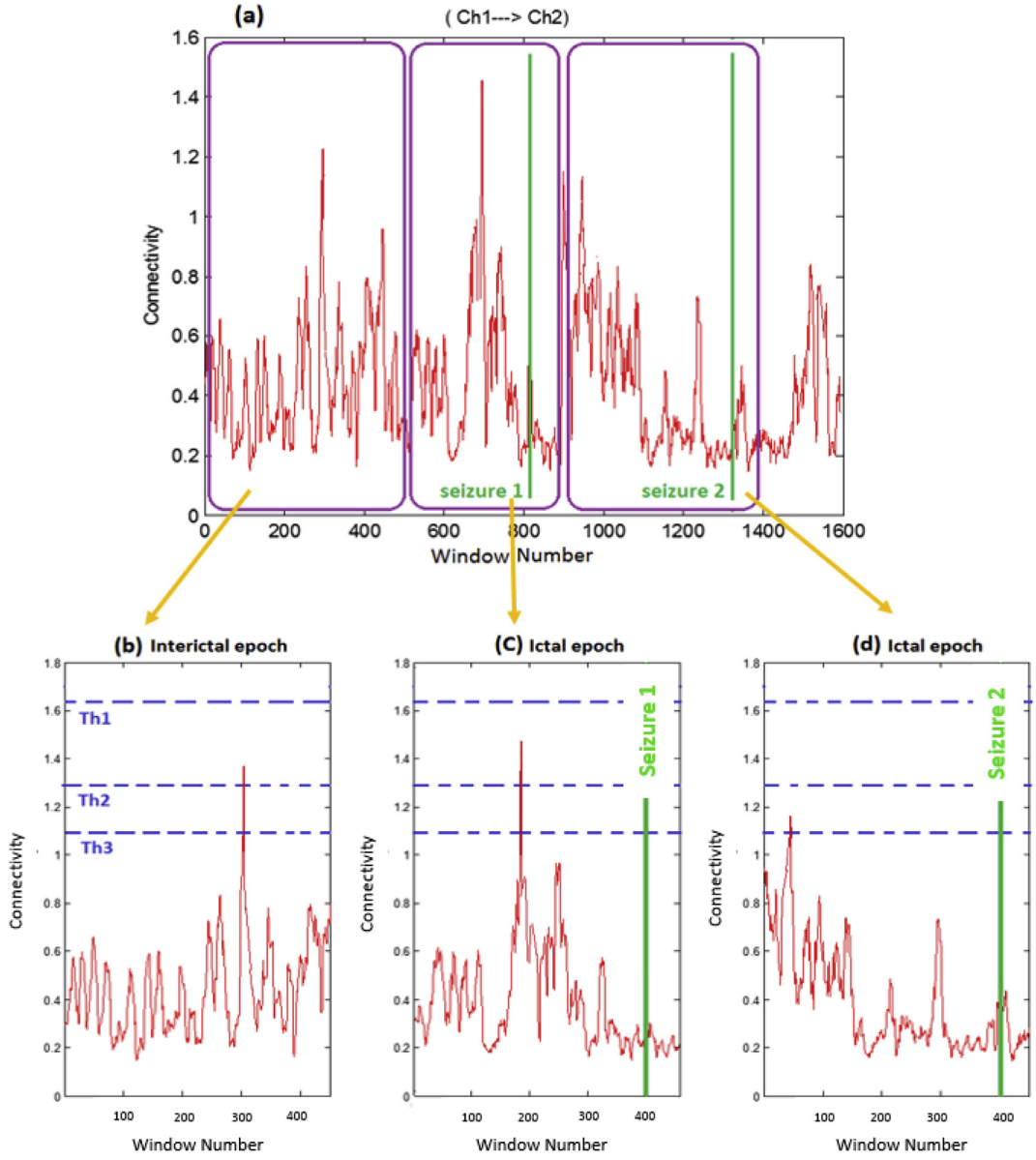

Fig. 13. Dependency between sensitivity and FPR; (a) the feature extracted by the proposed method; this feature has been shown for interictal epoch (b) and ictal epoch ((c) and (d)). The horizontal axis shows the window number which is considered 5 s. Vertical lines indicate seizure onsets. Three different thresholds show the dependency between sensitivity and FPR. For Th1, connectivity does not pass the threshold in either the "ictal" or "interictal" epoch. This means that in this case, sensitivity and FPR are zero. By considering Th2, the first seizure was predicted correctly (c) with the cost of one false prediction during the interictal epoch in (b). Decreasing the threshold to Th3 can predict the second seizure in (d).

results of the proposed method for the five patients of the Freiburg database.

Also, the FPR–Sensitivity diagram for these patients is presented in Fig. 15.

6. Discussion

In this paper, the RNN-NGUEW–GC method was analyzed by combining NGUEW for determination of the time lag, the RNN modeling, and the concept of GC. RNN-NGUEW-GC had good results in terms of both method accuracy and prediction of epileptic seizures.

In Section 5.1, we showed the performance of RNN-NGUEW-GC on different simulated data and evaluated our method, which is a generally adopted method in this field. In that section, the proposed method was applied to three different models of simulated data.

Let us start from the results of the first model, in section 5.1.1. In the simulations depicted in this section, an asymmetry is created, which is a unidirectional flow from x_2 to x_1, leading to an asymmetric causality in the appropriate direction. Fig. 7 illustrates the histogram of the resulting RNN-NGUEW-GC from 1000 surrogate datasets. In the surrogate test, a causal coupling will be concluded if and only if the connectivity of the original data (shown by a red star in Fig. 7) exceeds the threshold (see the Appendix). Consequently, Fig. 7 shows that only the $x_2 \rightarrow x_1$ connection exists in this model. Also, the results of using the "intensity of causality" index for estimating the strength of the interactions were shown in Table 2. The values of Table 2 show that the RNN-NGUEW-GC can estimate the strength of linear interactions with a low error.

Also in section 5.1.2, we illustrated a test based on a model with a time-varying coefficient to determine whether the proposed method has acceptable performance. The results presented in Fig. 8 show that RNN-NGUEW-GC has detected both the $x_2 \rightarrow x_1$ and the $x_1 \rightarrow x_2$ connections. Furthermore, Fig. 9 shows the time-varying coefficient corresponding

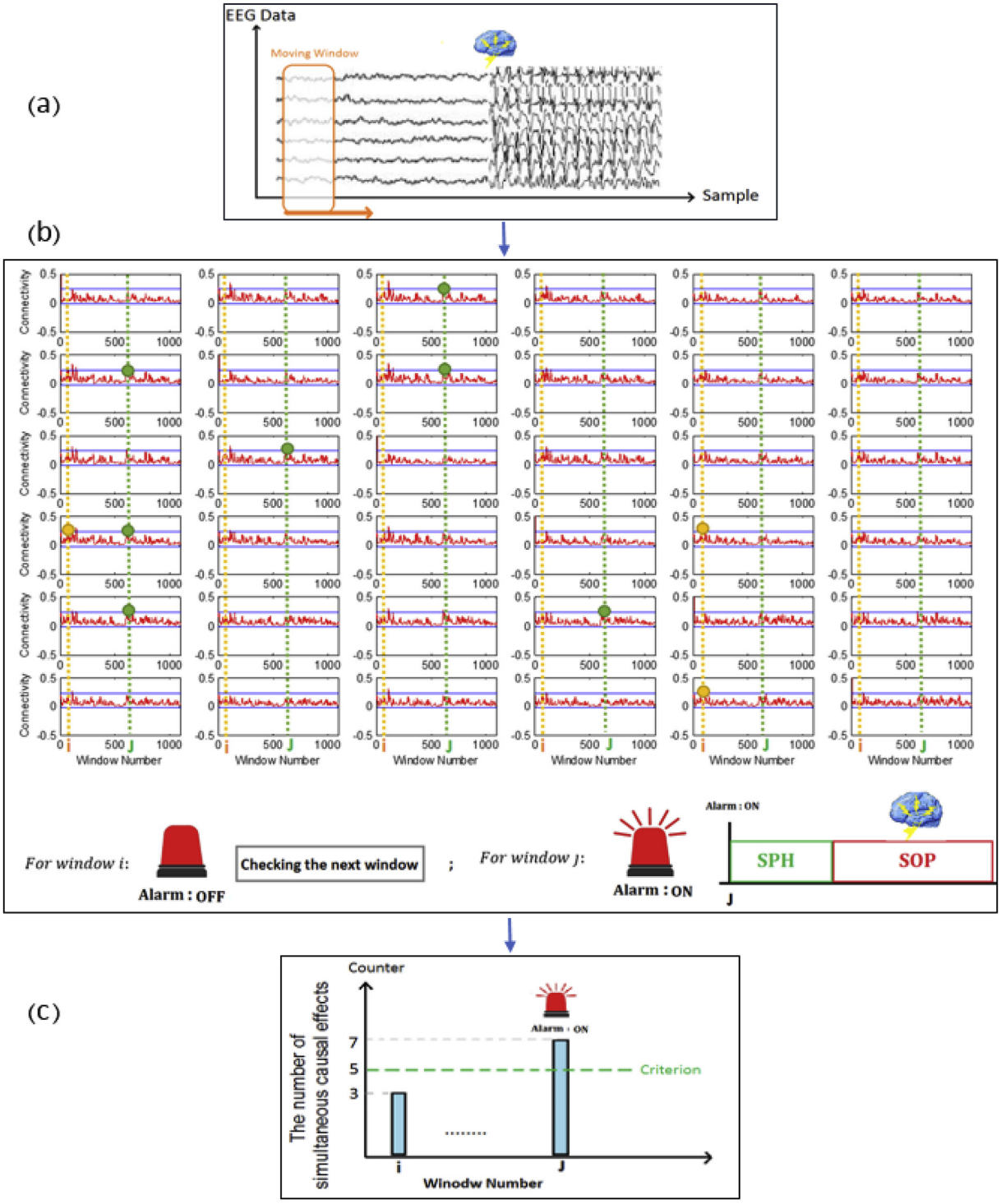

Fig. 14. Sample of decision-making for predicting epileptic seizures; (a) EEG data is shown before seizure and during it. Using the moving window, a few samples from EEG data were received for analysis every time. (b) Red curves: the connectivity variations among six channels for "ictal" and "interictal" data from patient number 8; blue horizontal lines: the thresholds; in each window, it checks how many times the connectivity passes the threshold. For window i, 3 out of 36 connectivities pass the threshold. Therefore, the alarm would not be triggered. For window j, 7 out of 36 connectivities pass the threshold. So, the alarm would be triggered. (c) The variable "Counter" shows in each window the number of connectivities passing the threshold. When "Counter" is greater than the criterion, the alarm will be triggered. For a correct prediction, a seizure onset must be after the SPH and within the SOP.

to the influence of $x_1\ (n-1)$ on $x_2(n)$. This figure proves that the estimated coefficient tracks the original value with a slight delay. Other time-invariant coefficients are shown in Table 3. These results suggest that the "intensity of causality" index can provide a sufficient approximation of these coefficients.

According to the results for the nonlinear and multivariate model illustrated in Fig. 10, RNN-NGUEW-GC correctly distinguishes direct connections from indirect connections. It detects $x_1 \rightarrow x_2$ and $x_2 \rightarrow x_3$ causal links and correctly does not find a connection from x_1 to x_3 . Also, the ability of our method was investigated in tracking an estimation of the strength of linear interactions for a nonlinear and multivariate model in Table 4.

Table 5
Results of five patients of the Freiburg database.

Patient NO	Number of seizure	Sensitivity	FPR
Patient 4	5	%100	0.1
Patient 8	2	%100	0.2
Patient 14	4	%100	0.3
Patient 15	4	%100	0.1
Patient 21	5	%100	0.2

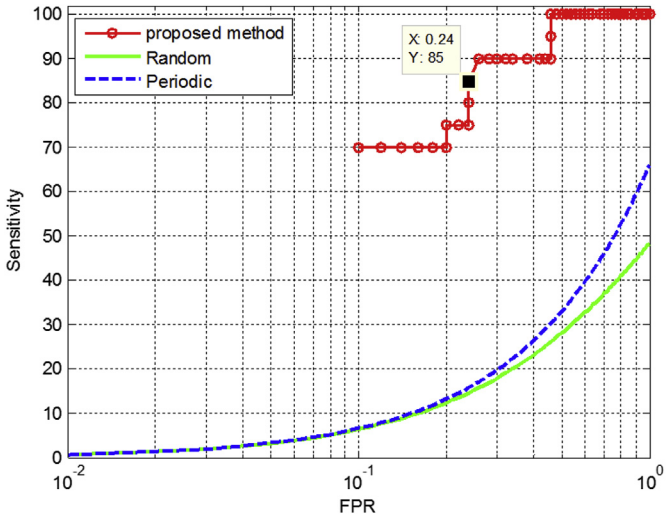

Fig. 15. FPR–Sensitivity diagram for all studied patients; high sensitivity plus low FRR for the red curve show the acceptable performance of the proposed method.

On the other hand, the proposed method is compared in this part with GC based on MVAR in the EEGLAB toolbox. In the EEGLAB toolbox, ARFIT for model fitting and the Akaike Criterion for model order estimation were used. Then, a model validation was performed with the investigation of whiteness, consistency, and stability. Finally, the connectivity estimation was obtained using GC. In Fig. 16, the results of comparison between the proposed method and the EEGLAB package is shown. The existence of effective connectivity between channels is indicated by '1' and the nonexistence of effective connectivity by '0'. Based on Fig. 16, the EEGLAB toolbox identifies the linear causal couplings but it is not capable of detecting nonlinear couplings (Fig. 16C), whereas the proposed method outperforms the EEGLAB package and identifies nonlinear links.

Also, EEGLAB does not indicate the intensity and strength of interactions between channels while in the proposed method, we defined an indicator called "intensity of causality" that estimates the strength of linear interactions with acceptable error. The results shown in Tables 2–4 prove this claim.

Epileptic seizure prediction results were reported in section 5.2. The results of Sensitivity and FPR for the patients were expressed in Table 5. An FPR equal to 0.1 means one false alarm in 10 h with a sensitivity of 100% for true alarms. Also, the area under the curve in Fig. 15 represents the performance of the proposed method as well as high sensitivity plus low FRR. It suggests high reliability in comparison with random, periodic predictors. It is expected that a prediction method provide us with significantly high sensitivity in comparison with unspecific methods, such as periodic and random methods. In random and periodic prediction methods, the EEG information is not used. Accordingly, the sensitivity calculation for them was based on the formula mentioned in Ref. [53].

The results were also compared to other studies in which the number of the patients was five or less. Nevertheless, it is complicated to tell which approach is the best since each approach was tested with one dataset. This comparison is provided in Table 6.

7. Conclusion

In this paper, a new method, called RNN-NGUEW-GC, was introduced for estimating effective connectivity. We combined the Neuron Growth Using Error Whiteness (NGUEW) algorithm, Recurrent Neural Network (RNN) modeling, and an index based on the concept of Granger causality (GC) to develop this method. In NGUEW, the proper time lag and self-organized network structure are obtained. Finding the correct time lag is very important for having a reliable estimation of effective connectivity. If the time lag is very high, the model overfits, whereby instabilities occur. On the other hand, if it is too low, the model cannot obtain the necessary dynamics of the data.

As far as we know, this is the first time that RNN and the neuron growth technique were used for effective connectivity estimation. The determination of a self-organized structure of the model and calculating the proper time lag are the superiorities of this method over multivariate auto-regressive methods. Therefore, we believe that the significant novelty of this study is its multi-technique integration of RNN and neuron growth plus the GC index for analyzing the effective connectivity. The performance of this approach was evaluated by applying this method to simulated data as well as to the prediction of epileptic seizures, yielding promising results.

As already mentioned, the indicator of "intensity of causality" in this study shows the strength of linear interactions, but it cannot

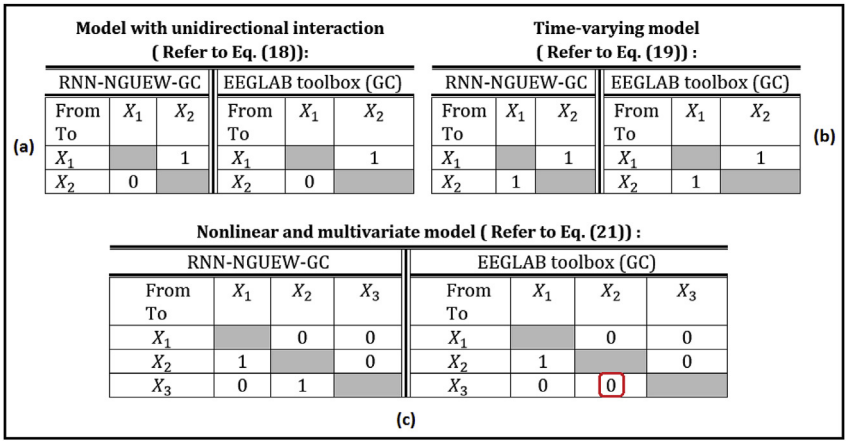

Fig. 16. The connectivity results of RNN-NGUEW-GC and EEGLAB for (a) Model with unidirectional interaction (b) Time-varying model (c) Nonlinear and multivariate model; in the nonlinear model, based on Eq. (21), there is a causal effect from x_2 to x_3. However, EEGLAB did not detect this connection.

Table 6
Some recent studies, compared with the proposed method.

Authors	year	Type of Recording	dataset	Classifier/method	patients	Sensitivity (%)	FPR (h^{-1})
Iasemidis et al. [54]	2005	iEEG	personal	–	2	81.82	0.15
Le Van Quyen et al. [55]	2005	iEEG	personal	_	5	70	n.m.
Direito et al. [56]	2011	scalp	EPILEPSIAE	mRMR		42.56***	n.m.
				RFE	3	39.61***	
				(NSGA-II)		47.89***	
Rabbi et al. [57]	2013	iEEG	EPILEPSIAE	–	1	80**	0.46**
Rasekhi et al. [58]	2013	iEEG	EPILEPSIAE	–	2	68.7	0.33
Keling Fei et al. [59]	2017	scalp	Hospital of Gansu and MIT epilepsy dataset	BPNN		83.75*	n.m.
				LDA	4	65.50*	
				KNN		69.50*	
This work	2018	iEEG	Freiburg	Connectivity using RNN	5	85	0.24

Scalp brain activity captured with surface electrodes; iEEG involves intracranial electrodes; EPILEPSIAE: European epilepsy database; n.m.: not mentioned; ***Average calculated for 3 subjects; ** sensitivity and FPR are reported for a preictal time of 45; * Average calculated for 2 features.

indicate the strength of nonlinear interactions. Indeed, this indicator is not applicable when the order of the Taylor series is greater than one. Therefore, the estimation of the strength of nonlinear interactions can be part of future studies. We believe that this would be an important task because with the calculation of the strength of nonlinear interactions we can estimate the nonlinear effect of each brain channel on the other channels before and after a seizure. In this way, we can consider these nonlinear effects for a more effective prediction of epileptic seizures and obtain better results.

Appendix

To evaluate the existence of causal effects, surrogate data are often generated. Surrogate datasets are made directly from the original dataset, where the statistical characteristics are preserved and the only difference is in their phase. Multiple methods have been suggested for generating surrogate datasets [60]. The method of surrogate dataset generation in this study is as follows:

1 Initially, the absolute value of the Fourier transform of the time series was calculated and then multiplied by a random phase that was symmetric. Finally, the inverse Fourier transformation was applied. Accordingly, surrogate data were generated just like a real signal with a different phase in comparison with the original data.
2 In order to achieve null distribution, after providing a sufficient number of surrogate data, the connectivity approximation method was applied. When Eq. (5) for the original data was greater than the threshold, there was a causal coupling. Note that the $(1 - P_{valu})$th percentile of this null distribution was considered as the threshold when it was positive; otherwise, the threshold was set to zero.

We repeated steps 1 and 2 for 1000 times in order to evaluate the significance of the obtained effective connectivity between all the channels.

Conflicts of interest

The authors declare that they have no conflict of interest.

Funding

This research did not receive any specific grant from funding agencies in the public, commercial, or not for profit sectors.

References

[1] V.K. Jirsa, A.R. McIntosh, Handbook of Brain Connectivity vol. 1, Springer, 2007.
[2] O. Sporns, G. Tononi, Structural Determinants of Functional Brain Dynamics, Handbook of Brain Connectivity, 2007, pp. 117–148.
[3] D. Poli, V.P. Pastore, P. Massobrio, Functional connectivity in in vitro neuronal assemblies, Front. Neural Circuits 9 (2015).
[4] C. Juan-Cruz, et al., Assessment of effective connectivity in Alzheimer's disease using granger causality, Converging Clinical and Engineering Research on Neurorehabilitation II, Springer, 2017, pp. 763–767.
[5] K. Alaerts, S.P. Swinnen, N. Wenderoth, Neural processing of biological motion in autism: an investigation of brain activity and effective connectivity, Sci. Rep. 7 (2017) 5612.
[6] B. Maharathi, J.A. Loeb, J. Patton, Estimation of resting state effective connectivity in epilepsy using direct-directed transfer function, Engineering in Medicine and Biology Society (EMBC), 2016 IEEE 38th Annual International Conference of the, IEEE, 2016.
[7] R.E. Rosch, et al., Imaging and Dynamic Causal Modelling Reveal Brain-wide Changes in Effective Connectivity and Synaptic Dynamics during Epileptic Seizures, bioRxiv, 2017, p. 160259.
[8] K.J. Friston, L. Harrison, W. Penny, Dynamic causal modelling, Neuroimage 19 (4) (2003) 1273–1302.
[9] L. Astolfi, et al., Estimation of the cortical connectivity by high-resolution EEG and structural equation modeling: simulations and application to finger tapping data, IEEE (Inst. Electr. Electron. Eng.) Trans. Biomed. Eng. 52 (5) (2005) 757–768.
[10] C.W. Granger, Investigating causal relations by econometric models and cross-spectral methods, Econometrica: J. Econom. Soc. (1969) 424–438.
[11] J. Burge, et al., Discrete dynamic Bayesian network analysis of fMRI data, Hum. Brain Mapp. 30 (1) (2009) 122–137.
[12] J.C. Rajapakse, J. Zhou, Learning effective brain connectivity with dynamic Bayesian networks, Neuroimage 37 (3) (2007) 749–760.
[13] X. Wu, J. Li, L. Yao, Determining effective connectivity from FMRI data using a Gaussian dynamic bayesian network, International Conference on Neural Information Processing, Springer, 2012.
[14] N. Talebi, A.M. Nasrabadi, I. Mohammad-Rezazadeh, Estimation of effective connectivity using multi-layer perceptron artificial neural network, Cognit. Neurodynamics (2017) 1–22.
[15] A. Khadem, G.-A. Hossein-Zadeh, Estimation of direct nonlinear effective connectivity using information theory and multilayer perceptron, J. Neurosci. Methods 229 (2014) 53–67.
[16] E. Koerner, H. Tsujino, T. Masutani, A cortical-type modular neural network for hypothetical reasoning, Neural Network. 10 (5) (1997) 791–814.
[17] R. Chandra, Competition and collaboration in cooperative coevolution of Elman recurrent neural networks for time-series prediction, IEEE Trans. Neural Network. Learn Syst. 26 (12) (2015) 3123–3136.
[18] A. Petrosian, et al., Recurrent neural network based prediction of epileptic seizures in intra-and extracranial EEG, Neurocomputing 30 (1–4) (2000) 201–218.
[19] J. Daunizeau, S.J. Kiebel, K.J. Friston, Dynamic causal modelling of distributed electromagnetic responses, Neuroimage 47 (2) (2009) 590–601.
[20] S.J. Kiebel, et al., Dynamic causal modeling for EEG and MEG, Hum. Brain Mapp. 30 (6) (2009) 1866–1876.
[21] M. Graña, L. Ozaeta, D. Chyzhyk, Dynamic causal modeling and machine learning for effective connectivity in auditory hallucination, Neurocomputing 326–327 (2017).
[22] W. Xiang, et al., A local adjustment strategy for the initialization of dynamic causal modelling to infer effective connectivity in brain epileptic structures, Comput. Biol. Med. 84 (2017) 30–44.
[23] N. Wiener, The theory of prediction, Modern mathematics for engineers 1 (1956) 125–139.
[24] S. Hu, H. Liang, Causality analysis of neural connectivity: new tool and limitations of spectral Granger causality, Neurocomputing 76 (1) (2012) 44–47.
[25] M.G. Tana, R. Sclocco, A.M. Bianchi, GMAC: a Matlab toolbox for spectral Granger causality analysis of fMRI data, Comput. Biol. Med. 42 (10) (2012) 943–956.
[26] M. Ding, Y. Chen, S.L. Bressler, 17 Granger Causality: Basic Theory and Application to Neuroscience. Handbook of Time Series Analysis: Recent Theoretical Developments and Applications, (2006), p. 437.
[27] M. Kamiński1, H. Liang, Causal influence: advances in neurosignal analysis, Crit. Rev. Biomed. Eng. 33 (4) (2005) 347–430.
[28] M.-H. Wu, R.E. Frye, G. Zouridakis, A comparison of multivariate causality based

measures of effective connectivity, Comput. Biol. Med. 41 (12) (2011) 1132–1141.
[29] M. Chávez, J. Martinerie, M. Le Van Quyen, Statistical assessment of nonlinear causality: application to epileptic EEG signals, J. Neurosci. Methods 124 (2) (2003) 113–128.
[30] D. Marinazzo, M. Pellicoro, S.J.P.r.l. Stramaglia, Kernel method for nonlinear Granger causality, 100 (14) (2008) 144103.
[31] D. Marinazzo, M. Pellicoro, S.J.P.r.E. Stramaglia, Kernel-Granger causality and the analysis of dynamical networks, 77 (5) (2008) p. 056215.
[32] S. Stramaglia, J.M. Cortes, D. Marinazzo, Synergy and redundancy in the Granger causal analysis of dynamical networks, New J. Phys. 16 (10) (2014) 105003.
[33] M. Farokhzadi, G.-A. Hossein-Zadeh, H.J.N. Soltanian-Zadeh, Nonlinear effective connectivity measure based on adaptive neuro fuzzy inference system and granger causality, 181 (2018) 382–394.
[34] H. Marko, The bidirectional communication theory–a generalization of information theory, IEEE Trans. Commun. 21 (12) (1973) 1345–1351.
[35] R. Vicente, et al., Transfer entropy—a model-free measure of effective connectivity for the neurosciences, J. Comput. Neurosci. 30 (1) (2011) 45–67.
[36] H. Choi, Localization and regularization of normalized transfer entropy, Neurocomputing 139 (2014) 408–414.
[37] C. McNorgan, M.F. Joanisse, A connectionist approach to mapping the human connectome permits simulations of neural activity within an artificial brain, Brain Connect. 4 (1) (2014) 40–52.
[38] C.M. Bishop, Neural Networks for Pattern Recognition, Oxford university press, 1995.
[39] Y. Qin, et al., A Dual-Stage Attention-Based Recurrent Neural Network for Time Series Prediction, (2017) 1704.02971.
[40] M. Jordan, Serial Order: a Parallel Distributed Processing Approach. Technical Report, June 1985-March 1986, California Univ., San Diego, La Jolla (USA), 1986 Inst. for Cognitive Science.
[41] J.L. Elman, Finding structure in time, Cogn. Sci. 14 (2) (1990) 179–211.
[42] H. Luo, S. Puthusserypady, Spatio-temporal modeling and analysis of fmri data using narx neural network, Int. J. Neural Syst. 16 (02) (2006) 139–149.
[43] H. Wang, G. Song, Innovative NARX recurrent neural network model for ultra-thin shape memory alloy wire, Neurocomputing 134 (2014) 289–295.
[44] K. Burse, R.N. Yadav, S. Shrivastava, Channel equalization using neural networks: a review, IEEE Trans. Syst. Man Cybern. Part C Appl. Rev. 40 (3) (2010) 352–357.
[45] H.-G. Han, S. Zhang, J.-F. Qiao, An adaptive growing and pruning algorithm for designing recurrent neural network, Neurocomputing 242 (2017) 51–62.
[46] H. Akaike, A new look at the statistical model identification, IEEE Trans. Autom. Control 19 (6) (1974) 716–723.
[47] B.L.P. Cheung, et al., Cross validation for selection of cortical interaction models from scalp EEG or MEG, IEEE (Inst. Electr. Electron. Eng.) Trans. Biomed. Eng. 59 (2) (2012) 504–514.
[48] T. Schneider, A. Neumaier, Algorithm 808: ARfit—a Matlab package for the estimation of parameters and eigenmodes of multivariate autoregressive models, ACM Trans. Math Software 27 (1) (2001) 58–65.
[49] T. Mullen, et al., An electrophysiological information flow toolbox for EEGLAB, Biol. Cybern. 83 (2010) 35–45.
[50] J. Geweke, Measurement of linear dependence and feedback between multiple time series, J. Am. Stat. Assoc. 77 (378) (1982) 304–313.
[51] Y. Zhao, et al., A new NARX-based Granger linear and nonlinear casual influence detection method with applications to EEG data, J. Neurosci. Methods 212 (1) (2013) 79–86.
[52] Database, Frieburg Seizure Prediction Database, (2007) http://epilepsy.uni-freiburg.de/freiburg-seizure-prediction-project/eeg-database.
[53] M. Winterhalder, et al., The seizure prediction characteristic: a general framework to assess and compare seizure prediction methods, Epilepsy Behav. 4 (3) (2003) 318–325.
[54] L. Iasemidis, et al., Long-term prospective on-line real-time seizure prediction, Clin. Neurophysiol. 116 (3) (2005) 532–544.
[55] M. Le Van Quyen, et al., Preictal state identification by synchronization changes in long-term intracranial EEG recordings, Clin. Neurophysiol. 116 (3) (2005) 559–568.
[56] B. Direito, et al., Optimized feature subsets for epileptic seizure prediction studies, Engineering in Medicine and Biology Society, EMBC, 2011 Annual International Conference of the IEEE, IEEE, 2011.
[57] A.F. Rabbi, L. Azinfar, R. Fazel-Rezai, Seizure prediction using adaptive neuro-fuzzy inference system, Engineering in Medicine and Biology Society (EMBC), 2013 35th Annual International Conference of the IEEE, IEEE, 2013.
[58] J. Rasekhi, et al., Preprocessing effects of 22 linear univariate features on the performance of seizure prediction methods, J. Neurosci. Methods 217 (1–2) (2013) 9–16.
[59] K. Fei, et al., Chaos feature study in fractional Fourier domain for preictal prediction of epileptic seizure, Neurocomputing 249 (2017) 290–298.
[60] K.T. Dolan, M.L. Spano, Surrogate for nonlinear time series analysis, Phys. Rev. 64 (4) (2001) p. 046128.